BNL-223507-2022-JAAM

Cost-Efficiency balanced polymer acceptors based on lowly fused Dithienopyrrolo[3, 2b]benzothiadiazole for 16.04% efficiency All-Polymer solar cells

C. Liao, R. Li

To be published in "Chemical Engineering Journal"

May 2022

Photon Sciences

Brookhaven National Laboratory

U.S. Department of Energy

USDOE Office of Science (SC), Basic Energy Sciences (BES) (SC-22)

DISCLAIMER

Cost-Efficiency Balanced Polymer Acceptors Based on Lowly Fused Dithienopyrrolo[3, 2b]benzothiadiazole for 16.04% Efficiency All-Polymer Solar Cells

Chentong Liao,[a] Yufei Gong,[a] Xiaopeng Xu,[a] Liyang Yu,[a] Ruipeng Li,[b] and Qiang Peng[a]**

[a] School of Chemical Engineering, Key Laboratory of Green Chemistry and Technology of Ministry of Education and State Key Laboratory of Polymer Materials Engineering, Sichuan University, Chengdu 610065, P. R. China

[b] National Synchrotron Light Source II, Brookhaven National Lab, Suffolk, Upton, NY 11973, USA

*To whom correspondence should be addressed: Tel: +86-28-85415506; fax: +86-28-85415506; email: liyangyu@scu.edu.cn; qiangpengjohnny@yahoo.com

Abstract

All-polymer solar cells (All-PSCs) constituted solely with polymeric semiconductor materials in the active layer, exhibit outstanding thermal stability and mechanical properties for potential large area and flexible applications in the future. The current prevailing polymer acceptors for most efficient All-PSCs are polymerized high-performance small molecule acceptor of Y6, *i.e.* the dithienothiopheno[3,2-b]-pyrrolobenzothiadiazole (BTTP) based polymers. However, the BTTP-based polymers often show relatively shallow highest occupied molecular orbital (HOMO) energy level and high figure of merit (FOM), which limit the rational selection of paring donor polymers. Herein, we presented two low-cost polymer acceptors, namely as BTP-T2F and BTP-2T2F, based on lowly fused dithienopyrrolo[3,2b]benzothiadiazole (BTP, removing two thiophene cycles from BTTP). The BTP-based polymers exhibited deeper HOMO levels around -5.90 eV, which could match variable donor polymers with low-lying HOMO levels, such as low-cost PTQ10. Additionally, the synthesis was significantly simplified compared to BTTP-based polymers. Highest power conversion efficiency (PCE) of 14.32% was achieved in binary blend device containing PTQ10:BTP-2T2F. By adding a miscibility-enhancing PBDTCl-TPD as a third component, the top PCE of 16.04% was obtained in ternary blend All-PSCs. Combining the high device performance and low estimated cost, extraordinary cost-efficiency balance was realized within these BTP-based polymer acceptors.

Keywords: all polymer solar cells; dithienopyrrolo[3,2b]benzothiadiazole; polymer acceptor; miscibility enhancer; cost-efficiency balance

1. Introduction

All polymer solar cells (All-PSCs) constituted solely with polymeric donor and acceptor materials in the active layer, exhibit outstanding thermal stability[1] and mechanical properties,[2] which make them suitable for large area and flexible solar cells in the future. Compared to the extensive research on electron-donating polymer donors,[3] investigation on constructing high-performance electron-accepting polymer acceptors stagnated behind. Excitingly, this filed advanced fast and attracted wide attention in the past few years.[4–6] The most straightforward strategy developed for constructing high-performance polymer acceptor is to connect high power conversion efficiency (PCE) small molecule acceptors, such as IDIC,[7] ITIC[8] and Y6[9], into the backbone of a conjugated polymer.[10]

As the Y6 series represent small molecular acceptors with highest PCEs at the moment, the recent emerging *n*-type polymer acceptors[4] based on the building block of dithienothiopheno[3,2-b]-pyrrolobenzothiadiazole (BTTP, typical core unit of Y6) show higher device performances compared to the earlier cases based on indacenodithiophene (IDT, typical core unit of IDIC; *e.g.* PZ1,[11] PFBDT-IDTIC[12] and PF2-DTSi[2]) and indacenodithienothiophene (IDTT, typical core units of ITIC; *e.g.* PN1[13] and PF3-DTCO[14]). This is because the significantly improved absorption of BTTP-based polymer acceptors at near infrared region, thanking for the sophisticated eight-ring BTTP structure with an electron accepting (A) core and two electron donating (D) wings fused to both sides. On the other hand, unlike solar cells containing small molecule acceptors, such as Y6, which operate efficiently with nearly 0 eV highest occupied molecular orbital (HOMO) offset,[15–17] there is no report so far on All-PSCs achieving such low HOMO offset. In practice, sufficient

HOMO offset (> 0.3 eV) is often required for All-PSCs to achieve efficient hole transferring at the donor/acceptor interface. This is why the donor polymer PM6 with relatively shallow HOMO level (E_{HOMO} = -5.65 eV)[18] (PM6 was mostly often used to blend with Y6[9] at present) was selected under compulsion for most polymer acceptors despite their much higher HOMO level than that of Y6 (E_{HOMO} = -5.65 eV).[4,5] Evidently, the reported BTTP-based polymer acceptors with low-lying HOMO levels showed superior solar cell performances because of the larger HOMO offset (related to the HOMO of PM6) enabled efficient hole transferring process when using PM6 as the donor polymer.[4,5] Hence, rational in further lowering the HOMO level of the polymerized small-molecule acceptors is of great interest, which will open opportunity for polymer acceptors to pair with high performance polymer donors with deeper HOMO levels than that of PM6, especially for low-cost donor polymer of PTQ10 (E_{HOMO} = -5.54 eV).[19] From this aspect, BTTP-based polymer acceptors with benzodithiophene (BDT) linkage group, such as PF5-Y5 (E_{HOMO} = -5.52 eV)[20] and PYN-BDTF (E_{HOMO} = -5.67 eV)[21], vinylene linkage group, such as PYV (E_{HOMO} = -5.61 eV)[22], thiophene linkage group, such as PYT (E_{HOMO} = -5.61 eV)[23] and PY5T (E_{HOMO} = -5.71 eV)[24], show rarely enough HOMO offset when paring with PTQ10. It is to be noticed that the regioregularity of these polymer acceptors played an interesting role on device performances.[25] The regioregular inward-positioned PYT, *i.e.* PY-IT[26–29], demonstrated significantly improved device performance owing to the improved intermolecular aggregation likely due to its packing style mimicking the unit cell of Y6.[30] The improved intermolecular aggregation was also found to provide a deeper E_{HOMO} for PY-IT (E_{HOMO} = -5.68 eV).[29]

Chemical modifications were also found with success in lowering the HOMO level of the BTTP-based polymer acceptors. PFY-3Se with two sulfur atoms in the

BTTP core replaced with selenium atoms was found with E_{HOMO} as deep as -5.65 eV.[31] Fluorination is another strategy to lower the E_{HOMO} for the high electron negativity of fluorine atoms.[25] Indeed, Y6 obtained its low-lying HOMO level partially due to the two fluorine substituents at each end groups, but the polymerization made such decoration challenging. By adding back one fluorine substituent back to the PY5T and PY-T polymers, PFA1[24] and PYF-T[32] achieved significantly deeper E_{HOMO} of -5.74 and -5.67 eV, respectively, thus significant increased the PCEs. The regioregular inward-position PYF-T, *i.e.* PYF-T-*o*, processed further lowered E_{HOMO} of -5.73 eV and improved device performance.[33] Two fluorinate substituents at each end group, which was equivalent to Y6, was achieved finally in polymer PY2F-T with E_{HOMO} at -5.71 eV, giving rise to an outstanding PCE reaching 15%.[34] Adopting electron deficient group as linkage is also an efficient approach to lower the E_{HOMO} of the polymer acceptors. For example, L14 with bithiophene imide linkage was found with low-lying E_{HOMO} at -5.79 eV.[35,36] Fluorination applied on the thiophene linkage group will also lower the HOMO level and promote PBTIC-*γ*-2T2F (with fluorinated bithiophene linkage) to demonstrate a E_{HOMO} of -5.56 eV.[25]

Despite above attempts, it is still of great challenge to further depress the E_{HOMO} of BTTP-based polymer lower than -5.80 eV. Therefore, we propose to eliminate two thiophene units from the BTTP core to design polymer acceptors based on the dithienopyrrole[3,2b]benzothiadiazolo (BTP) unit. The BTP unit constituted with the identical electron-withdrawing (A) benzothiadiazole unit as BTTP and two electron-donating (D) low-fused thienopyrrole wings from both sides. This six-fused-rings BTP maintained the DAD-type structural feature of BTTP and had already been explored for some applications in organic optoelectronics.[37,38] The elimination of electron-donating thiophene units was expected to increase the electron-accepting strength of the resulting polymers and significantly decrease the E_{HOMO}. Additionally, the smaller core is beneficial for intermolecular aggregation as large-fused-ring systems often tend to appear with distinguishable curvature.[30] Furthermore, with a low-fused core, the synthesis route of BTP-based polymers will be significantly simplified compared to the BTTP-based counterparts. The lowered E_{HOMO} makes it possible to pair with donor polymers with deeper HOMO levels, such as low-cost PTQ10.[19]

Herein, in this work, we designed and synthesized two regioregular BTP-based polymer acceptors, namely as BTP-T2F and BTP-2T2F (**Scheme 1**), with difluorothiophene and fluorinated bithiophene linkage groups, respectively. Removing two fused thiophene cycles and using fluorinated linkage groups were expected to benefit the lowering of the HOMO level and promoting the intermolecular aggregation. Finally, in binary blend All-PSCs, the PTQ10:BTP-2T2F device delivered a high PCE of 14.32% and exhibited a low figure of merit (FOM) of only 3.65. When a miscibility-enhancing benzodithiophene-based donor polymer PBDTCl-TPD was used as a third component, the PCE of 16.04% was realized in ternary blend All-PSCs, which is top efficiency value of All-PSCs at present.

2. Results and Discussion

2.1. Thermal Properties

Thermal properties of the two BTP-based polymers were investigated using thermogravimetric analysis (TGA) and differential scanning calorimetry (DSC) techniques. Both TGA thermograms (**Figure S1a**) of the two polymers showed clear step function with 5% weight loss observed at 337 ^{o}C for BTP-T2F and 350 ^{o}C for BTP-2T2F. Hence, both polymers show sufficient thermal stability within the typical temperature range of the processing and service. On the other hand, DSC thermograms (**Figure S1b**) did not reveal notable signatures for thermal transitions from 25 ^{o}C to 270 ^{o}C. The absence of detectable glass transitions can be a result of the relatively rigid polymer backbones.

2.2. Photophysical Properties

Photon absorbing ability of the two BTP-based polymers were examined using UV-vis absorption spectroscopy. In **Figure 1a**, the absorption spectrum of the BTP-T2F solution showed strong absorption band at 732 nm with maximum extinction coefficient reaching 1.71×10^5 M^{-1} cm^{-1}. On the other hand, the BTP-2T2F solution showed distinct absorption profile with significantly higher absorption around 550 nm and a high plateau stretching from 680 nm to 740 nm. This interesting absorption profile was confirmed in dilute solution of various concentrations. The maximum extinction coefficient of BTP-2T2F was found to be 1.54×10^5 M^{-1} cm^{-1}. The notably higher absorption of BTP-2T2F than BTP-T2F at 550 nm was confirmed by the absorption spectra of the thin films containing these two BTP-based polymers (**Figure 1b**). Interestingly, the solid-state absorption spectra of the two materials largely overlapped from 650 nm to 850 nm in thin films despite the difference in solution profiles, suggesting the plateau observed from the BTP-2T2F is likely due to some aggregation in solution. Similar absorption onsets were also extracted for the two BTP-based polymer at 830 nm for BTP-T2F and 839 nm for BTP-2T2F, corresponding to the optical bandgaps of 1.49 eV and 1.48 eV, respectively. The smaller bandgap for BTP-2T2F is beneficial for extending absorption range towards near infrared region. Compared to the absorption range of the donor polymer used in this work, *i.e.* PTQ10 and PBDTCl-TPD, the acceptors form complimentary absorption cover 450 nm to 800 nm wavelength range with over 50% of maximum extinction coefficient of at least one material.

2.3. Electrochemical Properties and Molecular Simulations

The energetic structures of the frontier orbitals of the two BTP-based polymers were further explored using cyclic voltammetry (CV) and compared to the donor materials. (**Figure 2a,b**) The energy diagram in **Figure 2c** summarized and compared the obtained energy levels of the HOMO and the lowest unoccupied molecular orbital (LUMO) of the semiconducting polymers used in this work. The BTP-T2F and BTP-2T2F were found with HOMO/LUMO levels at -4.03/-5.90 eV and -3.92/-5.87 eV, respectively. Both BTP-based polymers show significantly lower HOMO level than the BTTP-based polymers listed above, owing to the elimination of the two strong electron-donating thiophene rings. The low-lying HOMO level enabled these BTP-based polymers to be compatible to a broader range of polymer donors including PBDTCl-TPD (E_{HOMO} = -5.57 eV) and the cost efficient PTQ10 (E_{HOMO} = -5.61 eV).[19] The BTP-2T2F displayed a slightly higher LUMO level than that of the BTP-T2F due to the extra electron-donating thiophene unit, which is beneficial for obtaining a higher open circuit voltage (V_{oc}).

The energy levels obtained using CV method were supported by molecular simulations using density functional theory (DFT, at B3LYP/6-31G(d) level) (**Figure 3**). The calculated HOMO/LUMO energy levels for the BTP-T2F and BTP-2T2F were found at -5.69/-3.66 eV and -5.63/-3.59 eV, respectively. The lower calculated energy levels and narrower bandgap for BTP-T2F compared to BTP-2T2F agreed with the trend found in CV measurements. Interestingly, the spatial distributions of the frontier orbitals were significantly affected by the small change in linkage group. While the HOMO distribution of the BTP-T2F largely spreads over the BTP cores and the difluorothiophene linkage unit, it is predominately localized on the BTP core of BTP-2T2F. On the other hand, BTP-2T2F showed a more delocalized HOMO than BTP-T2F. One of the causes for the distinct HOMO and LUMO distribution between the two polymer acceptors is the molecular conformation. The front view of the calculated optimized molecular conformation showed that the in-plane dihedral angle between the two BTP units was significantly smaller for BTP-T2F (102.33^{o}) compared to BTP-2T2F (122.26^{o}). Meanwhile, the side view of the polymers showed larger out-of-plane dihedral angle for BTP-T2F (177.15^{o}) compared to BTP-2T2F (145.42^{o}). These differences suggested that the two fluorine atoms in the fluorobenzene linkage of the BTP-T2F enhanced planarization of the polymer backbone with intramolecular interaction. In a contrast, the inward facing fluorine atoms of the fluorinated bithiophene linkage of BTP-2T2F provided very limited restriction for conformational adjustment of the polymer backbone.

2.4. Photovoltaic Performances of All-PSCs

The photovoltaic performances of the BTP-based polymers were examined in binary blend All-PSCs parring with low-cost polymer donor PTQ10 in the conventional architecture of ITO/PEDOT:PSS/active layer/PNDIT-F3N/Ag. *J-V* characteristics of the top performing devices were presented in **Figure 4a** with the extracted photovoltaic parameters summarized in **Table 1**. The binary blend All-PSC devices suggested that both BTP-based polymers were compatible with PTQ10 by delivering decent PCEs. In comparison, the PTQ10:BTP-2T2T blend (PCE = 14.32%) notably outperformed PTQ10:BTP-T2F blend (PCE = 11.06%). The higher V_{oc} observed in devices containing BTP-2T2F (V_{oc} = 0.89 V) compared to those containing BTP-T2F (V_{oc} = 0.86 V) was expected for its higher LUMO level. Interestingly, remarkably higher short circuit current density (J_{sc}) was also found for BTP-2T2F-containing devices (J_{sc} = 23.15 mA cm^{-2}) compared to BTP-T2F-containing devices (J_{sc} = 19.01 mA cm^{-2}) despite the slightly higher maximum extinction coefficient obtained from BTP-T2F. The contrast in J_{sc} values was supported by the external quantum efficiency (EQE, **Figure 4b**) response from these devices. Indeed, higher EQE response was measured for BTP-2T2F device across the whole spectra. In the absorption range of the BTP-based polymers from 620 – 850 nm, the maximum EQE responses were found at 83% in the BTP-2T2F device compared to 67% in the BTP-T2F device. The drastic difference suggested that the photogenerated excitons in the BTP-T2F were not efficiently utilized. At the absorption range of PTQ10 from 420 – 620 nm, the BTP-2T2F-containing device also showed higher maximum EQE response (85% *vs* 74%). The more efficient exciton utilization of BTP-2T2F-containing device was further supported by its higher fill factor (FF = 69.5%) compared to the device containing BTP-T2F (FF = 65.2%).

BTP-2T2F was selected as the polymer acceptor for constructing ternary blend All-PSCs due to its superior photovoltaic performances. The device architecture and fabrication method of the ternary blend All-PSCs were identical to the binary blend devices. The total donor and acceptor ratio (1:1.2 wt%) was kept unchanged, and the total donor concentration was kept at 20 mg mL^{-1}. **Figure 4c** presented the *J-V* characteristics of the ternary blends with PTQ10:PBDTCl-TPD ratio denoted in the figure. The photovoltaic parameters of the ternary blends obtained from the *J-V* curves were summarized in **Table 1**. The V_{oc} showed a slight decrease from 0.89 V to 0.88 V when PTQ10 was replaced by PBDTCl-TPD gradually. This was due to the slightly higher HOMO level of PBDTCl-TPD than PTQ10. A clear bell shape was observed in J_{sc} with the maximum reaching 23.91 mA cm^{-2} at 40% of PBDTCl-TPD and gradually drop to 22.54 mA cm^{-2} with 100% PBDTCl-TPD as the donor material.

The EQE response confirmed the J_{sc} with integrated current J_{EQE} within its proximity with identical trend (**Figure 4d**). As the absorption range for the two donor polymers large overlapped, the EQE responses covered identical ranges. It is noticed, when PBDTCl-TPD was added to the blend, the EQE response increased at all wavelengths with similar EQE response profile, suggesting increased utilization efficiency of exciton generated in both donor and acceptors. When more than 40% PTQ10 was replaced by PBDTCl-TPD, EQE response started to drop at lower wavelength where the donor polymers absorbed strongly while the EQE response where BTP-2T2F absorption remained high. This suggested that the lower extinction coefficient was the main cause for the J_{sc} drop at high content of PBDTCl-TPD. The FF also followed the bell trend with its maximum value reached 75.4% after adding 40% of PBDTCl-TPD. The highest PCE of 16.04% was realized finally at 40% of PBDTCl-TPD due to the highest J_{sc} and FF.

To further highlight the outstanding performances of BTP-based polymers at a potential low cost, the commercialization potential of the binary blend devices were compared to some state-of-the-art All-PSCs with an established method.[39–41] The cost-efficiency balance of an active layer combination is assessed with a figure of merit (FOM = ASC/PCE, where ASC is the average synthesis complexity). The ASC is an average value of synthesis complexity (SC) of donor (SC_D) and acceptor (SC_A) used in the active layer normalized to their weight percentages. The estimation of SC takes in contribution from synthesis steps, yield, purification steps and hazardous chemicals used in various steps.[39] **Table 2** presents the comparison in PCE and FOM between the binary blend ALL-PSCs systems listed in Figure 1. The IDT-based polymers show relatively low PCE around 10% with a high FOM of 5.62 by PZ1 partially due to the high SC_A. PFBDT-IDTIC also displayed a very high SC_A raised by the complex synthesis of the benzodithiophene unit, which led to a FOM as high as 7.50. The IDTT based polymers with extended fused ring core showed a notably increased SC_A as expected. However, the PCE was not found to increase significantly due to the extended absorption was compromised by the lowered V_{oc} when paring with PM6. Consequently, the FOM values for PN1 and PF3-DTCO based devices were both over 6. The BTTP-based polymers show significantly improved PCE due to the extended photon absorption. Despite the SC_A values even surpassed Y6 (SC_A = 70)[41], the relatively high PCE lowered the FOMs for regioregular fluorinated PYF-T-*o* (FOM = 4.99) and PT-2FT (FOM = 4.99).[42] However, both BTP-based polymers in this work show notably lower SC_A values under 70 due to the shortened fused core.[9] More importantly, the lower energy levels enabled them to be matched with low-cost polymer donor of PTQ10, which displayed an outstanding SCA of 27.65 compared to 73.05 for PM6.[41] With comparable PCE with the top performing BTTP-based polymers, BTP-2T2F displayed an ultra-low FOM of 3.65 which is by far the lowest FOM value for All-PSCs and is one of the lowest values among all organic solar cells.[41]

2.5. Thin Film Morphology Studies

A common challenge for achieving high-performance All-PSCs is the high phase separation tendency between the polymers, which often leads to oversized phase separated domains to limit the utilization of photogenerated excitons. The strong contrast in photovoltaic performances between the binary blend devices containing these two BTP-based polymers can be caused by differences in thin film morphology due to the dissimilar conformational freedom suggested by the DFT simulations. For this reason, the thin film morphologies were studied using atomic force microscopy (AFM, **Figure 5**). From the AFM images of thin films containing the binary blends, rough surface (root mean square of surface height, RMS = 0.58 nm) with many large aggregates can be found in both height and phase images from the binary blend thin film containing BTP-T2F. In a clear contrast, much fewer aggregates were scattered on the surface of the binary thin film containing BTP-2T2F with lower roughness (RMS = 0.45 nm). Hence, the stronger phase separation in PTQ10:BTP-T2F was accused from the lower performing All-PSCs. The origin for the higher tendency for phase separation in PTQ10:BTP-T2F can be caused by poorer miscibility. Indeed, the surface energy (γ) for PTQ10, BTP-T2F and BTP-2T2F were found at 27.9, 38.3 and 36.6 mJ m^{-2}, respectively, *c.f.* **Figure S2** for surface energy measurements. The interaction factor ($\chi = (\sqrt{\gamma_1} - \sqrt{\gamma_2})^2$)[43] estimated for the PTQ10:BTP-T2F and PTQ10:BTP-2T2F blends were 0.82 and 0.59, respectively, suggesting stronger phase separation in the PTQ10:BTP-T2F blend which may cause the low J_{sc} and FF.

The AFM images suggested that the number of aggregates were further reduced in the ternary blend with an RMS reduced to 0.40 nm suggesting the phase separation was further suppressed. This is likely due to the surface energy of PBDTCl-TPD (31.9 mJ m^{-2}) lies between those of PTQ10 and BTP-2T2F. The χ values for the PTQ10:PBDTCl-TPD and PBDTCl-TPD:BTP-2T2F blends were calculated to be 0.13 and 0.16, respectively, suggesting that the PBDTCl-TPD was more miscible with both PTQ10 and BTP-2T2F. The addition of PBDTCl-TPD with intermediate surface energy into immiscible blend of PTQ10:BTP-2T2F can be illustrated in a classical ternary miscibility phase diagram (**Figure 6a**), where the miscibility limits of two immiscible liquids can be suppressed by the addition of a third compound which is miscible with the two.[44] A good example is the miscibility limit of water and oil can be achieved at lower temperature in the presence of an organic acid.[45–47] It was more evident in the phase diagram (**Figure 6b**) which showed the addition of PBDTCl-TPD suppressed the miscibility limits. Moving from binary blend into the ternary blend, homogeneous liquid phase was preserved at a higher concentration during the solvent evaporation in solution processing. As illustrated in the schematic in **Figure 6c**, liquid-liquid phase separation appeared for the binary PTQ10:BTP02T2F blend due to the poor miscibility at increasing solution concentration during solution process, while the solubility enhancing PBDTCl-TPD maintained the solution in one phase. The delayed liquid-liquid phase separation would significantly limit the formation of large-scale phase separation in solid state thin films. Therefore, the additional PBDTCl-TPD can be used to weaking phase separation between PTQ10 and BTP-2T2F.

The nanostructures of the thin films were further studied using grazing-incidence wide-angle X-ray scattering (GIWAXS, **Figure 7**). The neat BTP-based polymers showed similar face-on configurations on the substrates with (100) lamellar stacking diffraction and (001) diffraction in-plane and (010) π-stacking diffraction out-of-plane. Interestingly, BTP-T2F showed a (100) diffraction at a higher q_{100} = 3.00 nm^{-1} (d_{100} = 2.09 nm) and a (001) diffraction at a lower q_{001} =5.18 nm^{-1} (d_{001} = 1.21 nm) compared to BTP-2T2F, which showed its (100) diffraction at q_{100} = 2.83 nm^{-1} (d_{100} = 2.22 nm) and (001) diffraction at q_{001} =5.45 nm^{-1} (d_{001} = 1.15 nm). This observation agreed with the molecular configuration where the BTP-T2F showed a higher dihedral angle in-plane, which squeezed the molecule along its backbone axis and widened the molecule sideways. The flatter molecular configuration of BTP-T2F led to a tighter π-stacking (q_{010} = 18.14 nm^{-1}, d_{010} = 0.346 nm) compared to BTP-2T2F (q_{010} = 18.06 nm^{-1}, d_{010} = 0.348 nm). Interestingly, the BTP-T2F displayed slightly lower diffraction intensities compared to BTP-2T2F despite its flatter molecular configuration possibly due to the molecular interlock restricted the polymer into a conformation not favorable for intermolecular aggregation.

Because the donor polymers were also found in face-on configuration (**Figure 7** and **Figure S3**) with diffractions close to the diffractions of the acceptor polymers, it is challenging to decouple the diffraction intensity contribution from the donor or acceptor materials in the blends. The diffraction patterns were found very similar in all blend films. However, it could be noticed that the intensity of (010) diffraction decreased when PBDTCl-TPD was added into the system. As the diffraction intensity from neat PBDTCl-TPD thin film was not significantly lower, it was suggested that the addition of PBDTCl-TPD enhanced the miscibility of the amorphous phase of the polymers, which limited the crystallization of the active layer blend.

2.6. Charge Transport and Recombination Processes

To determine the structure-property-performance relationship of the All-PSCs, charge transport and recombination processes of the binary and ternary thin films were studied. The charge carrier transport mobilities of the blend thin films were characterized using space charge limited current (SCLC) method (**Figure 8a,b**). The hole and electron mobility (μ_h/μ_e) of the PTQ10:BTP-T2F, PTQ10:BTP-2T2F, and ternary blend with 40% PBDTC-TPD in PBDTC-TPD:BTP-2T2F were found to be $1.75 \times 10^{-4}/5.41 \times 10^{-5}$, $2.43 \times 10^{-4}/1.02 \times 10^{-4}$, $4.30 \times 10^{-4}/2.25 \times 10^{-4}$ and $2.26 \times 10^{-4}/8.34 \times 10^{-5}$ cm^2 V^{-1} s^{-1}, with μ_h/μ_e ratios of 3.23, 2.38, 1.91 and 2.71, respectively. Interestingly, the binary blend containing BTP-2T2F showed higher mobilities and more balanced charge transport compared to the one containing BTP-T2F, which agreed with its higher crystallinity. In the ternary blend, further increase in mobilities with more balanced charge transport were observed. This supported the notably increased J_{sc} and FF in the ternary blends.

The recombination processes were also affected by the thin film morphologies. The plot **Figure 8c** illustrated the photocurrent density (J_{ph}) *vs* effective voltage (V_{eff}), where the J_{ph} is the difference between the light and dark current density and the V_{eff} is the difference between the applied voltage and the applied voltage where the light and dark currents are equal. The ternary blend with 40% BTP-3T2F showed a significant higher J_{ph} at low effectively voltages and reached the plateau at a lower V_{eff}. These observations have already suggested a more efficient charge generation process than the binary blend devices. The charge dissociation probability ($P_{E,T}$), which was estimated by the ratio between the maximum J_{ph} divided by the J_{ph} of the plateau, also showed higher value for the ternary blend (97.8%) than the binary blends (96.5%, 97.3% and 97.1% for PTQ10:BTP-T2F, PTQ10:BTP-2T2F and PBDTC-TPD:BTP-2T2F, respectively).

The recombination process of the top performing All-PSCs were further evaluated. **Figure 8c,d** displayed the V_{oc} and J_{sc} evolution at various incidence light intensity (P_{light}), where the slop kT/q was extracted from the former and an exponent α was fitted to $J_{sc} \propto P_{light}^{\alpha}$ based on the later. The kT/q and α values were found at 1.46/0.978, 1.29/0.989, 1.17/0.995 and 1.34/0.984 for PTQ10:BTP-T2F, PTQ10:BTP-2T2F, ternary blend with 40% PBDTC-TPD or PBDTC-TPD:BTP-2T2F, respectively. The kT/q close to 1 suggested the dominance of bimolecular recombination and the higher α value suggested lower amount of bimolecular recombination events. Hence, the lower kT/q and higher α value found in the ternary blend suggested slowest recombination process in the corresponding devices, which supported the highest FF.

3. Conclusions

In this work, two relatively low-cost BTP-based polymer acceptors of BTP-T2F and

BTP-2T2F were designed and synthesized for All-PSCs. These polymer acceptors are based on a lowly fused BTP unit compared to the BTTP core of Y6 used commonly for main current high-performance polymer acceptors. The BTP core significantly lowered the HOMO levels of the polymer acceptors, increased the electron accepting strength and enabled them to pair with variable donor polymers with low-lying HOMO levels, especially for low-cost PTQ10. PCE of 14.32% was achieved in the binary blend devices based on PTQ10:BTP-2T2F. When a miscibility-enhancing donor polymer PBDTC-TPD was added into the mixture and the resulting ternary blend devices realized a champion PCE of 16.04% when 40% of PTQ10 was replaced by PBDTC-TPD, which is a top efficiency value of All-PSC at present. Importantly, the BTP-based polymer showed outstanding cost-efficiency balance with a very good FOM value of 3.65, which is the lowest one for All-PSCs and one of the lowest cases for organic solar cells up to now. This work demonstrated the potential of BTP-based polymer acceptors for low-cost but high-performance All-PSCs. Additionally, miscibility enhancer was introduced as a useful tool for tuning the morphology of the ternary blend All-PSCs.

4. Experimental Section

4.1. Materials and Synthesis

The detailed synthesis routes of the two BTP-based polymer acceptors were presented in Supporting Information. The molecular weight (M_n) and polydispersity (PDI) values were measured to be 17.1 kDa, 21.8 kDa and 2.33, 2.13 for BTP-T2F and BTP-2T2F, respectively.

4.2. Materials Characterization

The ^{1}H and ^{13}C NMR spectra were measured with a Bruker Avance-400 spectrometer. *d*-Chloroform was used as the solvent and tetramethyl silane (TMS) was used as the internal standard. Molecular weights of the polymers were determined using a Waters 1515 gel permeation chromatography (GPC). UV-vis absorption spectra were measured with a Shimadzu UV-2700 spectrophotometer. CV measurements were conducted with a CHI660 potentiostat/galvanostat electrochemical workstation with a scanning rate of 50 mV s^{-1}. AFM images were taken in tapping mode with a Bruker Innova scanning probe microscope. Surface energies were measured using a KRÜSS DSA100 drop shape analyzer with water and diiodomethane as testing liquids. GIWAXS measurements were performed at Complex Materials Scattering (CMS) beamline of the National Synchrotron Light Source II (NSLS-II), Brookhaven National Lab.

4.3. Fabrication of All-PSC devices

Conventional architecture of ITO/PEDOT:PSS/active layer/ PNDIT-F3N/Ag was used for evaluation of the All-PSCs in this work. The active layers were fabricated by spin coating from a chloroform solution (20 mg mL^{-1} in total solid content, total donor:acceptor ratio of 1:1.2, with 1 vol% 1-chloronaphthalene (CN) solvent additive). Thermal annealing (110 ^{o}C for 10 min) was performed on all devices. Hole only and electron only devices for SCLC measurements were fabricated similarly to the All-PSCs. All device fabrication and measurements were performed in an argon gas filled glove box except the deposition of PEDOT:PSS. The *J-V* characteristics were recorded with a Keithley 2400 SMU and a SAN-EI XES-70S1 solar simulator. The EQE responses were recorded with an Enlitech QE-R solar quantum efficiency testing system in air.

Declaration of Competing Interest

The authors declare that they have no known competing financial interests or personal relationships that could have appeared to influence the work reported in this paper.

Acknowledgements

This work was supported by the National Natural Science Foundation of China (NSFC, 21825502, 22075190, 21905185 and 22105135), Special funds for local science and technology development guided by the central government (2020ZYD004), the Foundation of State Key Laboratory of Polymer Materials Engineering (SKLPME 2017-2-04) and the Fundamental Research Funds for the Central Universities. The authors thank Yanping Huang from Center of Engineering Experimental Teaching, School of Chemical Engineering, Sichuan University for the help of NMR measurements. The authors also thank National Synchrotron Light Source II (NSLS-II, Contract No. DE-SC0012704) Brookhaven National Laboratory for providing GIWAXS experiment time.

References

[1] Q. Fan, W. Su, S. Chen, T. Liu, W. Zhuang, R. Ma, X. Wen, Z. Yin, Z. Luo, X. Guo, L. Hou, K. Moth-Poulsen, Y. Li, Z. Zhang, C. Yang, D. Yu, H. Yan, M. Zhang, E. Wang, *Angew. Chem. Int. Ed.* **2020**, *59*, 19835.

[2] Q. Fan, W. Su, S. Chen, W. Kim, X. Chen, B. Lee, T. Liu, U. A. Méndez-Romero, R. Ma, T. Yang, W. Zhuang, Y. Li, Y. Li, T. S. Kim, L. Hou, C. Yang, H. Yan, D. Yu, E. Wang, *Joule* **2020**, *4*, 658.

[3] X. Xu, L. Yu, Q. Peng, *Chin. J. Chem.* **2021**, *39*, 243.

[4] Q. Fan, Z. Xiao, E. Wang, L. Ding, *Sci. Bull.* **2021**, *66*, 1950.

[5] B. Wu, B. Yin, C. Duan, L. Ding, *J. Semicond.* **2021**, *42*, 080301.

[6] Z. Zhang, Y. Li, *Angew. Chem. Int. Ed.* **2021**, *60*, 4422.

[7] Y. Lin, Q. He, F. Zhao, L. Huo, J. Mai, X. Lu, C. J. Su, T. Li, J. Wang, J. Zhu, Y. Sun, C. Wang, X. Zhan, *J. Am. Chem. Soc.* **2016**, *138*, 2973.

[8] W. Zhao, D. Qian, S. Zhang, S. Li, O. Inganäs, F. Gao, J. Hou, *Adv. Mater.* **2016**, *28*, 4734.

[9] J. Yuan, Y. Zhang, L. Zhou, G. Zhang, H. L. Yip, T. K. Lau, X. Lu, C. Zhu, H. Peng, P. A. Johnson, M. Leclerc, Y. Cao, J. Ulanski, Y. Li, Y. Zou, *Joule* **2019**, *3*, 1140.

[10] Q. Wei, W. Liu, M. Leclerc, J. Yuan, H. Chen, Y. Zou, *Sci. Chin. Chem.* **2020**, *63*, 1352.

[11] Z.-G. G. Zhang, Y. Yang, J. Yao, L. Xue, S. Chen, X. Li, W. Morrison, C. Yang, Y. Li, *Angew. Chem. Int. Ed.* **2017**, *56*, 13503.

[12] H. Yao, F. Bai, H. Hu, L. Arunagiri, J. Zhang, Y. Chen, H. Yu, S. Chen, T. Liu, J. Y. L. Lai, Y. Zou, H. Ade, H. Yan, *ACS Energy Lett.* **2019**, *4*, 417.

[13] J. Wu, Y. Meng, X. Guo, L. Zhu, F. Liu, M. Zhang, *J. Mater. Chem. A* **2019**, *7*, 16190.

[14] Q. Fan, R. Ma, T. Liu, W. Su, W. Peng, M. Zhang, Z. Wang, X. Wen, Z. Cong, Z. Luo, L. Hou, F. Liu, W. Zhu, D. Yu, H. Yan, E. Wang, *Sol. RRL* **2020**, *4*, 1.

[15] Z. H. Chen, P. Q. Bi, X. Y. Yang, M. S. Niu, K. N. Zhang, L. Feng, X. T. Hao, *J. Phys. Chem. C* **2019**, *123*, 12676.

[16] T. Saito, S. Natsuda, K. Imakita, Y. Tamai, H. Ohkita, *Sol. RRL* **2020**, *4*, 2000255.

[17] Y. Cai, H. Zhang, L. Ye, R. Zhang, J. Xu, K. Zhang, P. Bi, T. Li, K. Weng, K. Xu, J. Xia, Q. Bao, F. Liu, X. Hao, S. Tan, F. Gao, X. Zhan, Y. Sun, *ACS Appl. Mater. Interfaces* **2020**, *12*, 43984.

[18] M. Zhang, X. Guo, W. Ma, H. Ade, J. Hou, *Adv. Mater.* **2015**, *27*, 4655.

[19] C. Sun, F. Pan, H. Bin, J. Zhang, L. Xue, B. Qiu, Z. Wei, Z. Zhang, Y. Li, *Nat. Commun.* **2018**, *9*, 743.

[20] Q. Fan, Q. An, Y. Lin, Y. Xia, Q. Li, M. Zhang, W. Su, W. Peng, C. Zhang, F. Liu, L. Hou, W. Zhu, D. Yu, M. Xiao, E. Moons, F. Zhang, T. D. Anthopoulos, O. Inganäs, E. Wang, *Energy Environ. Sci.* **2020**, *13*, 5017.

[21] N. Su, R. Ma, G. Li, T. Liu, L. W. Feng, C. Lin, J. Chen, J. Song, Y. Xiao, J. Qu, X. Lu, V. K. Sangwan, M. C. Hersam, H. Yan, A. Facchetti, T. J. Marks, *ACS Energy Lett.* **2021**, *6*, 728.

[22] X. Zhao, T. Wang, W. Wang, R. Sun, Q. Wu, H. Shen, J. Xia, Y. Wang, M. Zhang, J. Min, *Polymer* **2021**, *230*, 124104.

[23] Q. Wu, W. Wang, Y. Wu, Z. Chen, J. Guo, R. Sun, J. Guo, Y. (Michael) Yang, J. Min, *Adv. Funct. Mater.* **2021**, *31*, 2010411.

[24] F. Peng, K. An, W. Zhong, Z. Li, L. Ying, N. Li, Z. Huang, C. Zhu, B. Fan, F. Huang, Y. Cao, *ACS Energy Lett.* **2020**, *5*, 3702.

[25] H. Wang, H. Chen, W. Xie, H. Lai, T. Zhao, Y. Zhu, L. Chen, C. Ke, N. Zheng, F. He, *Adv. Funct. Mater.* **2021**, *31*, 2100877.

[26] T. Liu, T. Yang, R. Ma, L. Zhan, Z. Luo, G. Zhang, Y. Li, K. Gao, Y. Xiao, J. Yu, X. Zou, H. Sun, M. Zhang, T. A. Dela Peña, Z. Xing, H. Liu, X. Li, G. Li, J. Huang, C. Duan, K. S. Wong, X. Lu, X. Guo, F. Gao, H. Chen, F. Huang, Y. Cao, B. Tang, H. Yan, *Joule* **2021**, *5*, 914.

[27] H. Fu, Y. Li, J. Yu, Z. Wu, Q. Fan, F. Lin, H. Y. Woo, F. Gao, Z. Zhu, A. K. Y. Jen, *J. Am. Chem. Soc.* **2021**, *143*, 2665.

[28] R. Ma, J. Yu, T. Liu, G. Zhang, Y. Xiao, Z. Luo, G. Chai, Y. Chen, Q. Fan, W. Su, G. Li, E. Wang, X. Lu, F. Gao, B. Tang, H. Yan, *Aggregate* **2021**, DIO: 10.1002/agt2.58.

[29] Z. Luo, T. Liu, R. Ma, Y. Xiao, L. Zhan, G. Zhang, H. Sun, F. Ni, G. Chai, J. Wang, C. Zhong, Y. Zou, X. Guo, X. Lu, H. Chen, H. Yan, C. Yang, *Adv. Mater.* **2020**, *32*, 2005942.

[30] L. Zhu, M. Zhang, G. Zhou, T. Hao, J. Xu, J. Wang, C. Qiu, N. Prine, J. Ali, W. Feng, X. Gu, Z. Ma, Z. Tang, H. Zhu, L. Ying, Y. Zhang, F. Liu, *Adv. Energy Mater.* **2020**, *10*, 1904234.

[31] Q. Fan, H. Fu, Q. Wu, Z. Wu, F. Lin, Z. Zhu, J. Min, H. Y. Woo, A. K. Y. Jen, *Angew. Chem. Int. Ed.* **2021**, *60*, 15935.

[32] H. Yu, Z. Qi, J. Yu, Y. Xiao, R. Sun, Z. Luo, A. M. H. Cheung, J. Zhang, H. Sun, W. Zhou, S. Chen, X. Guo, X. Lu, F. Gao, J. Min, H. Yan, *Adv. Energy Mater.* **2021**, *11*, 2003171.

[33] H. Yu, M. Pan, R. Sun, I. Agunawela, J. Zhang, Y. Li, Z. Qi, H. Han, X. Zou, W. Zhou, S. Chen, J. Y. L. Lai, S. Luo, Z. Luo, D. Zhao, X. Lu, H. Ade, F.

Huang, J. Min, H. Yan, *Angew. Chem. Int. Ed.* **2021**, *60*, 10137.

[34] R. Sun, W. Wang, H. Yu, Z. Chen, X. X. Xia, H. Shen, J. Guo, M. Shi, Y. Zheng, Y. Wu, W. Yang, T. Wang, Q. Wu, Y. (Michael) Yang, X. Lu, J. Xia, C. J. Brabec, H. Yan, Y. Li, J. Min, *Joule* **2021**, *5*, 1548.

[35] H. Sun, H. Yu, Y. Shi, J. Yu, Z. Peng, X. Zhang, B. Liu, J. Wang, R. Singh, J. Lee, Y. Li, Z. Wei, Q. Liao, Z. Kan, L. Ye, H. Yan, F. Gao, X. Guo, *Adv. Mater.* **2020**, *32*, 2004183.

[36] B. Liu, H. Sun, J. W. Lee, J. Yang, J. Wang, Y. Li, B. Li, M. Xu, Q. Liao, W. Zhang, D. Han, L. Niu, H. Meng, B. J. Kim, X. Guo, *Energy Environ. Sci.* **2021**, *14*, 4499.

[37] K. J. Kass, M. Forster, U. Scherf, *Angew. Chem. Int. Ed.* **2016**, *55*, 7816.

[38] Z. S. Huang, H. L. Feng, X. F. Zang, Z. Iqbal, H. Zeng, D. B. Kuang, L. Wang, H. Meier, D. Cao, *J. Mater. Chem. A* **2014**, *2*, 15365.

[39] R. Po, G. Bianchi, C. Carbonera, A. Pellegrino, *Macromolecules* **2015**, *48*, 453.

[40] J. Min, Y. N. Luponosov, C. Cui, B. Kan, H. Chen, X. Wan, Y. Chen, S. A. Ponomarenko, Y. Li, C. J. Brabec, *Adv. Energy Mater.* **2017**, *7*, 1700465.

[41] J. Xiao, X. Jia, C. Duan, F. Huang, H. Yip, Y. Cao, *Adv. Mater.* **2021**, *33*, 2008158.

[42] M. Schlosser, C. Heiss, *Eur. J. Org. Chem.* **2003**, *2003*, 4618.

[43] H. Feng, Y. Yi, X. Ke, J. Yan, Y. Zhang, X. Wan, C. Li, N. Zheng, Z. Xie, Y. Chen, *Adv. Energy Mater.* **2019**, *9*, 1803541.

[44] D. F. Othmer, W. S. Bergen, N. Shlechter, P. F. Bruins, *Ind. Eng. Chem.* **1945**,

37, 890.

[45] D. Laiadi, A. Hasseine, A. Merzougui, *Fluid Phase Equilib.* **2012**, *313*, 114.

[46] H. Ghanadzadeh, A. Ghanadzadeh Gilani, K. Bahrpaima, R. Sariri, *J. Chem. Thermodyn.* **2010**, *42*, 267.

[47] S. Şahin, Ş. Ismail Kirbaşlar, M. Bilgin, *J. Chem. Thermodyn.* **2009**, *41*, 97.

Legends for Schemes, Figures and Tables

Scheme 1. Chemical structure, blended donor, power conversion efficiency (PCE) and figure of merit (FOM) of the polymer acceptors in recent high-performance all-PSCs. a,b) Polymer based on ladder-tape small molecular acceptor unit. c) Polymer based on Y6-tape small molecular acceptor unit. d) Polymer based on low fused Y6-tape small molecular acceptor unit (this work).

Figure 1. a) UV-vis absorption spectra of the two BTP-based polymer in solution. b) Normalized UV-vis absorption spectra of thin films containing each of the semiconducting polymers used in this work.

Figure 2. a,b) Cyclic voltammograms (CV) of the polymer donors (a) and acceptors (b) used in this work. c) Energy diagram summarizing the energy levels of the frontier molecular orbitals of the semiconducting polymer used in this work based on the CV measurements.

Figure 3. Simulated molecular conformation and distribution of frontier molecular orbitals of the BTP-based polymers with respective energy levels.

Figure 4. *J-V* characteristics (a,c) and EQE responses (b,d) of the top performing binary (a,b) and ternary (c,d, PTQ10:PBDTCl-TPD ratio was denoted in the figures) All-PSCs.

Figure 5. AFM height and phase images of thin films containing the binary and ternary blends.

Figure 6. Three dimensional (a) and two dimensional (b) phase diagrams illustrating the miscibility limited evolution of binary and ternary blends with miscibility enhancer. (c) Schematic illustrating the nanostructure evolution during the solution process.

Figure 7. a) GIWAXS images of neat and blended polymer thin films. b) in-plane and out-of-plane line cuts from (a)

Figure 8. a,b) SCLC characterization for hole only (a) and electron only (b) devices. c-e) Plots illustrating J_{ph}-V_{eff} (c), V_{oc}-P_{light} (d) and J_{sc}-P_{light} (e) relationships of the top performing All-PSCs.

Table 1. Photovoltaic parameters of the top performing binary and ternary (PTQ10:PBDTCl-TPD:BTP-2T2F) All-PSCs.

Table 2. Estimation of the FOM comparing this work to top performing binary All-PSCs.

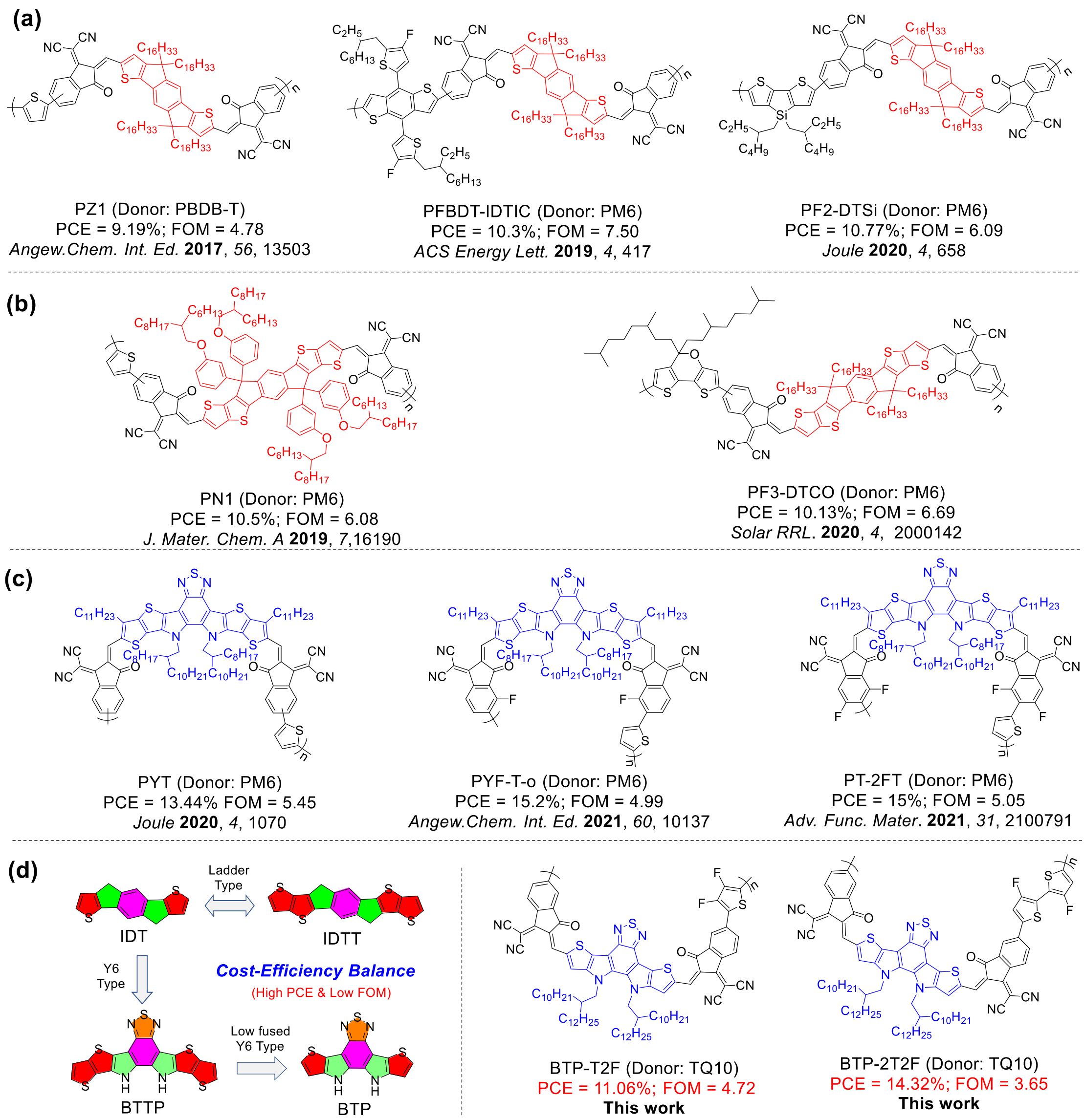

Scheme 1. Chemical structure, blended donor, power conversion efficiency (PCE) and figure of merit (FOM) of the polymer acceptors in recent high-performance all-PSCs. a,b) Polymer based on ladder-tape small molecular acceptor unit. c) Polymer based on Y6-tape small molecular acceptor unit. d) Polymer based on low fused Y6-tape small molecular acceptor unit (this work).

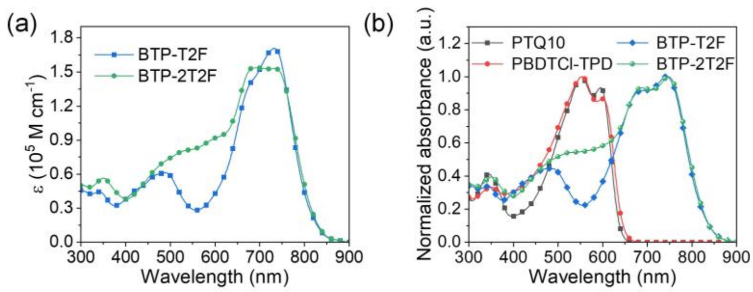

Figure 1. a) UV-vis absorption spectra of the two BTP-based polymer in solution. b) Normalized UV-vis absorption spectra of thin films containing each of the semiconducting polymers used in this work.

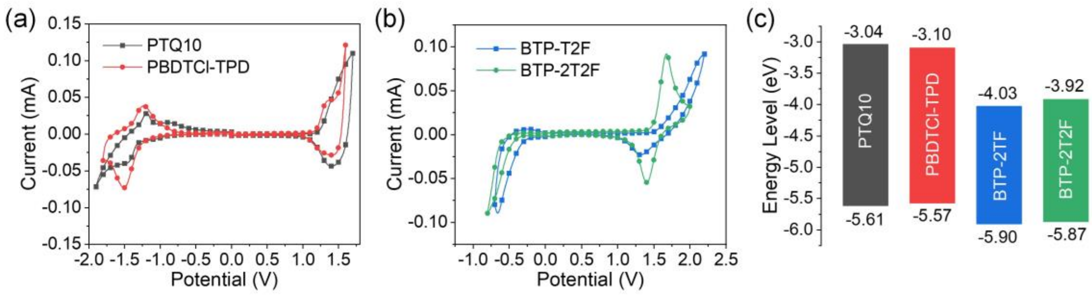

Figure 2. a,b) Cyclic voltammograms (CV) of the polymer donors (a) and acceptors (b) used in this work. c) Energy diagram summarizing the energy levels of the frontier molecular orbitals of the semiconducting polymer used in this work based on the CV measurements.

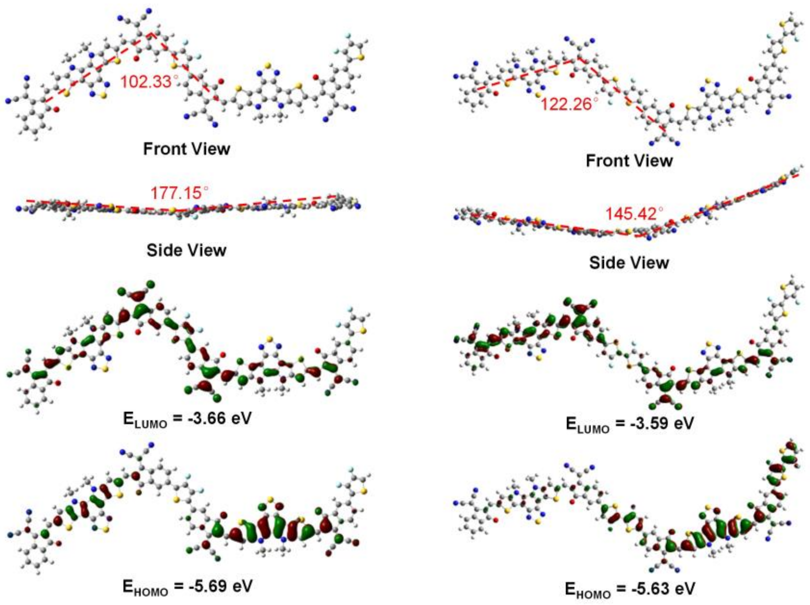

Figure 3. Simulated molecular conformation and distribution of frontier molecular orbitals of the BTP-based polymers with respective energy levels.

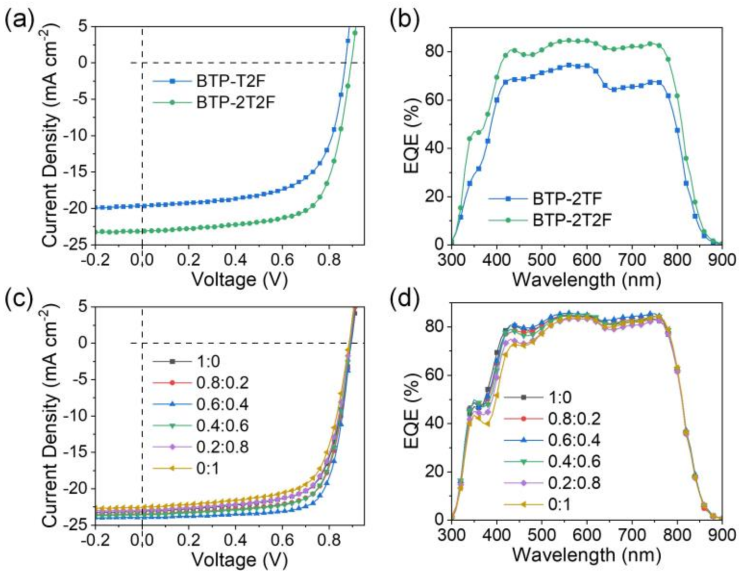

Figure 4. *J-V* characteristics (a,c) and EQE responses (b,d) of the top performing binary (a,b) and ternary (c,d, PTQ10:PBDTCl-TPD ratio was denoted in the figures) All-PSCs.

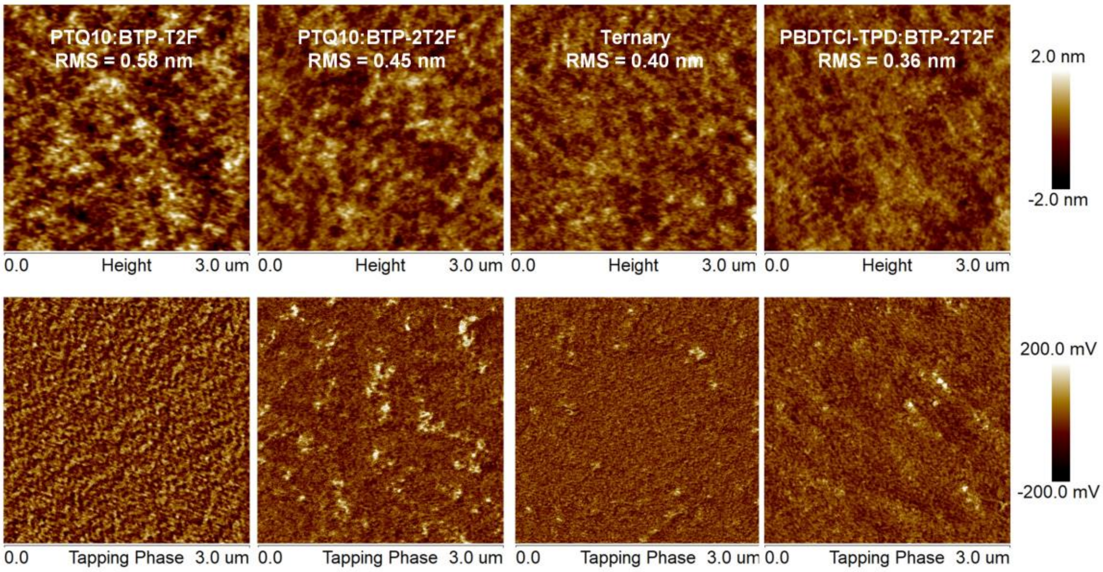

Figure 5. AFM height and phase images of thin films containing the binary and ternary blends.

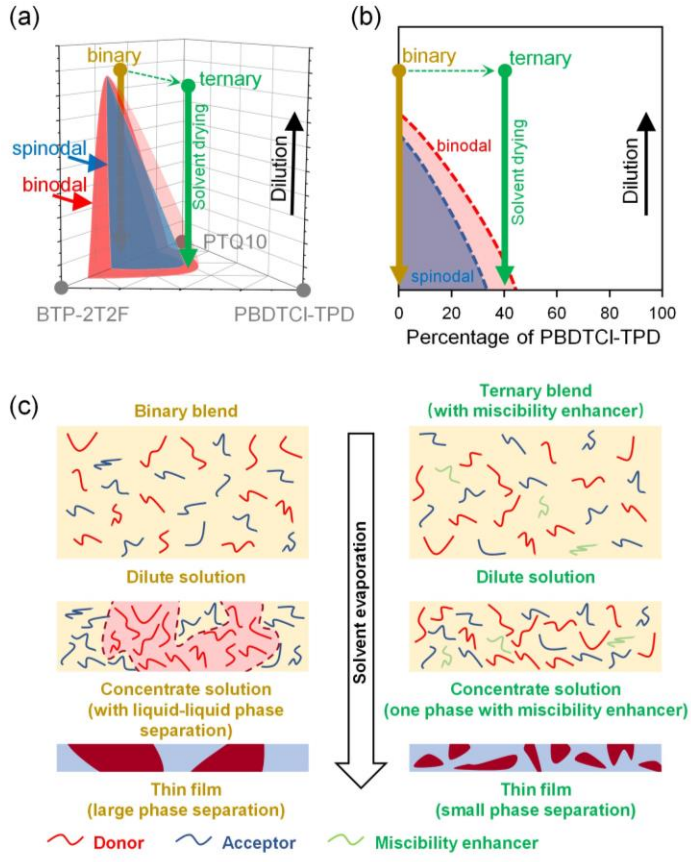

Figure 6. Three-dimensional (a) and two-dimensional (b) phase diagrams illustrating the miscibility limited evolution of binary and ternary blends with miscibility enhancer. (c) Schematic illustrating the nanostructure evolution during the solution process.

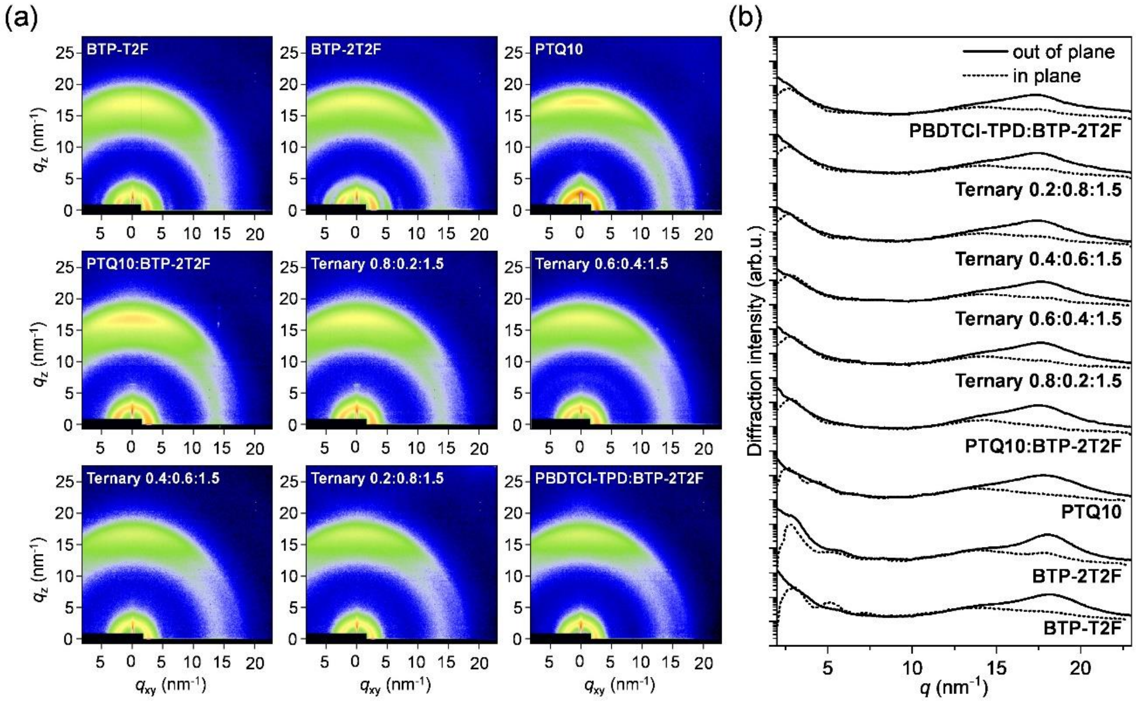

Figure 7. a) GIWAXS images of neat and blended polymer thin films. b) in-plane and out-of-plane line cuts from (a)

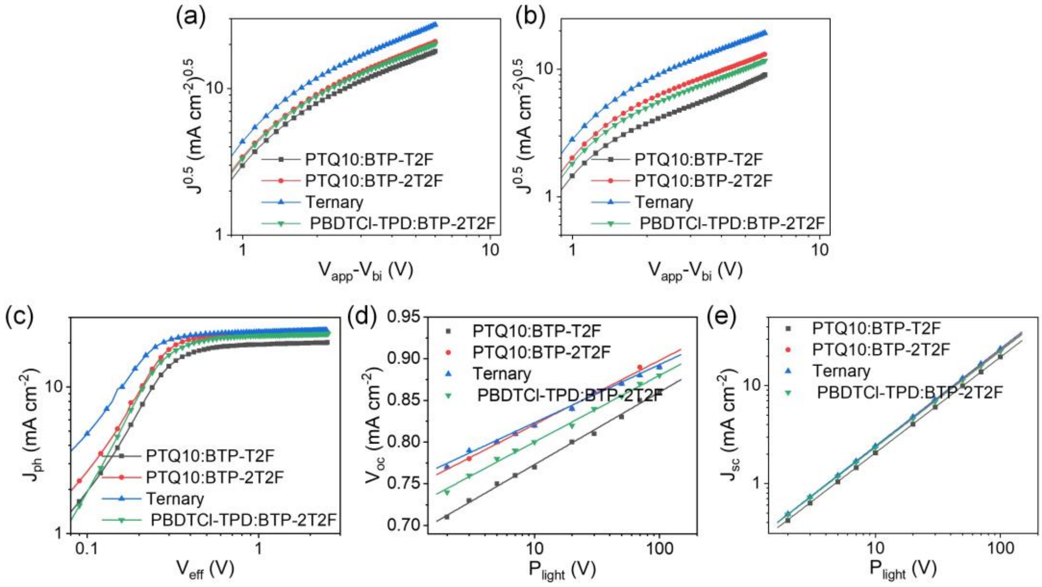

Figure 8. a,b) SCLC characterization for hole only (a) and electron only (b) devices. c-e) Plots illustrating J_{ph}-V_{eff} (c), V_{oc}-P_{light} (d) and J_{sc}-P_{light} (e) relationships of the top performing All-PSCs.

Table 1. Photovoltaic parameters of the top performing binary and ternary (PTQ10:PBDTCl-TPD:BTP-2T2F) All-PSCs.

Active blends	V_{oc} (V)	J_{sc} (mA cm^{-2})	J_{EQE} (mA cm^{-2})	FF (%)	PCE (%)
PTQ10:BTP-T2F	0.86	19.58	19.01	65.2	11.06
PTQ10:BTP-2T2F	0.89	23.15	22.54	69.5	14.32
Ternary (0.8:0.2:1.2)	0.89	23.49	22.83	72.3	15.12
Ternary (0.6:0.4:1.2)	0.89	23.91	23.21	75.4	16.04
Ternary (0.4:0.6:1.2)	0.88	23.56	22.89	72.8	15.09
Ternary (0.2:0.8:1.2)	0.88	22.92	22.28	70.6	14.24
PBDTCl-TPD:BTP-2T2F	0.88	22.54	21.89	68.6	13.61

Table 2. Estimation of the FOM comparing this work to top performing binary All-PSCs.

Polymer acceptor	Paring donor	SC_D	SC_A	Top PCE (%)	FOM	ref
PZ1	PM6	73.05	45.17	11.2	5.62	[11]
PFBDT-IDTIC	PM6	73.05	83.58	10.3	7.50	[12]
PF2-DTSi	PM6	73.05	50.82	10.77	6.09	[2]
PN1	PM6	73.05	50.11	10.5	6.08	[13]
PF3-DTCO	PM6	73.05	57.2	10.13	6.69	[14]
PYT	PM6	73.05	73.29	13.44	5.45	[23]
PYF-T-*o*	PM6	73.05	78.15	15.2	4.99	[33]
PT-2FT	PM6	73.05	77.6	15	5.05	[34]
BTP-T2F	PTQ10	27.65	68.62	14.32	3.65	This work
BTP-2T2F	PTQ10	27.65	68.56	11.06	4.72	This work

Supporting Information

Cost-Efficiency Balanced Polymer Acceptors Based on Lowly Fused Dithienopyrrolo[3, 2b]benzothiadiazole for 16.04% Efficiency All-Polymer Solar Cells

Chentong Liao,[a] Yufei Gong,[a] Xiaopeng Xu,[a] Liyang Yu,[a] Ruipeng Li,[b] and Qiang Peng[a]**

[a] School of Chemical Engineering, Key Laboratory of Green Chemistry and Technology of Ministry of Education and State Key Laboratory of Polymer Materials Engineering, Sichuan University, Chengdu 610065, P. R. China

[b] National Synchrotron Light Source II, Brookhaven National Lab, Suffolk, Upton, NY 11973, USA

*To whom correspondence should be addressed: Tel: +86-28-85415506; fax: +86-28-85415506; email: liyangyu@scu.edu.cn; qiangpengjohnny@yahoo.com

1. Materials

5,6-Dinitro-4,7-di(thiophen-2-yl)benzo[c][1,2,5]thiadiazole (**1**)[1] and 2-(5-bromo-3-oxo-2,3-dihydro-1H-inden-1-ylidene)malononitrile (**4**)[2] were synthesized according to literature reports. Other reagents, solvent and materials were purchased from commercial sources and used as received.

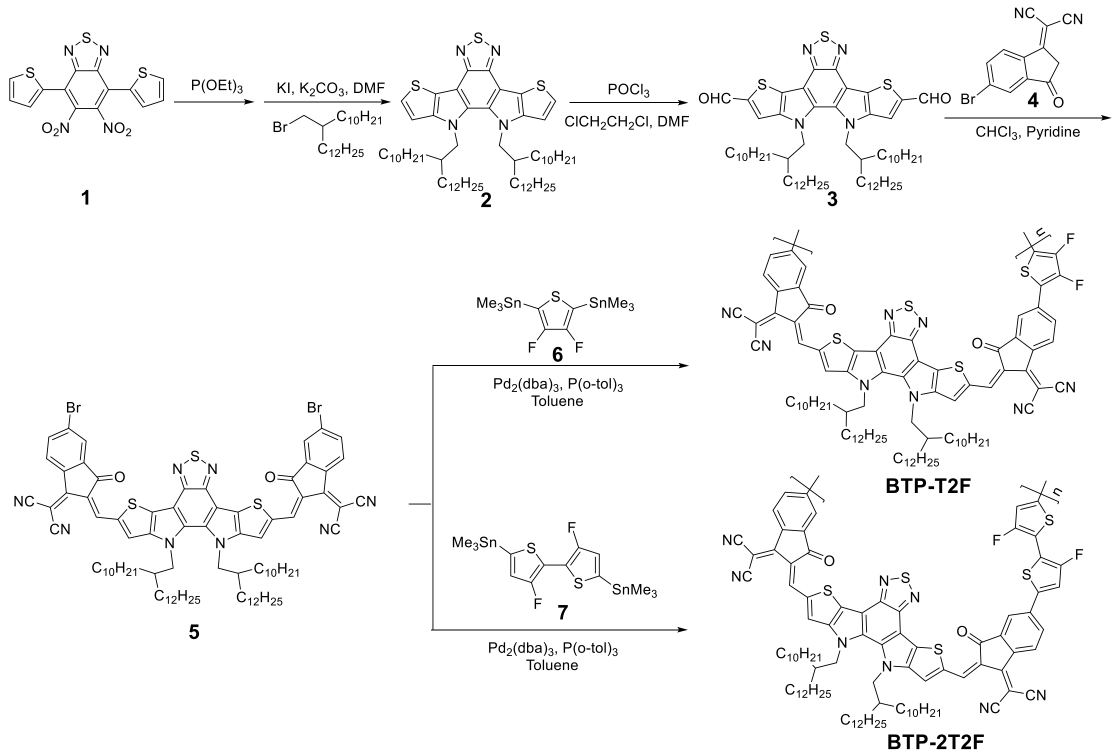

Scheme S1. Synthesis route of the two BTP-based polymers

2. Synthesis Details

Synthesis of compound 2

Add triethyl phosphite (21.0 mL, 120.00 mmol) into compound 1 (1.56g, 4.00 mmol) in a 100 mL flask. Stir at 190 °C in argon atmosphere for 16 h. After cooling down to room temperature, evaporate solvent with elevated temperature and reduced pressure. In this mixture, add 11-(bromomethyl)tricosane (16.70 g, 40.00 mmol), potassium iodide (1.00 g, 6.00 mmol), Potassium carbonate (3.32 g, 24.00 mmol), N,N-dimethylformamide (15.0 mL) sequentially. Stir at 110 ^{o}C for 12 h. After cooling down to room temperature, extract with dichloromethane, dry over anhydrous magnesium sulfate and evaporate under reduced pressure. The pure product of compound 2 was obtained as light green liquid by column chromatography with petroleum ether as the eluent (0.56 g, 14%). ^{1}H NMR (400 MHz, $CDCl_3$, δ /ppm): 7.41 (d, *J* = 5.2 Hz, 2H), 7.15 (d, *J* = 5.2 Hz, 2H), 4.48 (d, *J* = 7.7 Hz, 4H), 1.99 (m, 2H), 1.30 – 0.70 (m, 92H). ^{13}C NMR (101 MHz, $CDCl_3$, δ /ppm): 147.60, 145.15, 132.83, 126.43, 121.22, 112.00, 110.66, 54.38, 37.95, 32.30, 31.95, 31.70, 30.51, 29.65, 29.16, 27.19, 25.60, 22.70, 14.14. HR-MS (MALDI-TOF) $[M+H]^+$ calcd. for ($C_{62}H_{103}N_4S_3^+$): 999.7339; found: 999.7362.

Synthesis of compound 3

In a 100 mL three neck flask, add compound 2 (1.70 g, 1.70 mmol), N,N-dimethylformamide (3.3 mL) and 1,2-dichloroethane (25.0 mL). Add phosphorus oxychloride (3.2 mL, 34.00 mmol) dropwise into the flask at 0 oC under argon atmosphere. Stir at 0 ^{o}C for 1 h and 65 ^{o}C for 12 h, sequentially. Pour the obtained mixture into 300 mL water with sufficient sodium bicarbonate to remove excess phosphorus oxychloride. Stir the mixture for 2 h, extract with dichloromethane, dry over anhydrous magnesium sulfate and evaporate under reduced pressure. The pure product of compound 3 was obtained as orange solid by column chromatography with petroleum ether/dichloromethane as the eluent (v/v, 1:1) (1.53 g, 85%). ^{1}H NMR (400 MHz, $CDCl_3$, δ /ppm): 10.02 (s, 2H), 7.83 (s, 2H), 4.54 (d, *J* = 7.6 Hz, 4H), 2.00 (m, 2H), 1.30 – 0.70 (m, 92H). ^{13}C NMR (101 MHz, $CDCl_3$, δ /ppm): 182.96, 147.43, 144.79, 144.58, 134.74, 128.43, 119.62, 112.24, 54.69, 38.37, 31.93, 31.88, 30.51, 29.64, 29.29, 25.60, 22.68, 14.13. HR-MS $[M+H]^+$ calcd. for ($C_{64}H_{103}N_4O_2S_3^+$): 1055.7238; found: 1055.7071.

Synthesis of compound 5

In a 50 mL flask, add compound 3 (1.70 g, 1.70 mmol), compound 4 (0.26 g, 0.94 mmol), chloroform (15.0 mL) and pyridine (1.0 mL), sequentially. Stir at 50 oC for 24 h under argon atmosphere. After cooling down to room temperature, wash the mixture in methanol. The pure product of compound 4 was obtained as dark blue solid by column chromatography with petroleum ether/dichloromethane as the eluent (v/v, 3:2) (0.06 g, 77%). ^1H NMR (400 MHz, $CDCl_3$, δ /ppm): 8.85 (s, 2H), 8.49 (d, *J* = 8.4 Hz, 2H), 7.97 (d, *J* = 1.8 Hz, 2H), 7.89 (s, 2H), 7.78 (dd, *J* = 8.4, 1.9 Hz, 2H), 4.58 (d, *J* = 7.6 Hz, 4H), 2.19 (m, 2H), 1.30 – 0.70 (m, 92H). ^{13}C NMR (101 MHz, $CDCl_3$, δ /ppm): 186.04, 159.17, 147.36, 146.66, 140.10, 138.47, 138.46, 138.30, 137.71, 136.10, 135.85, 129.84, 126.93, 126.44, 126.02, 122.47, 114.62, 113.66, 69.53, 55.07, 38.49, 31.93, 31.91, 30.62, 29.83, 29.35, 25.84, 22.68, 14.10, HR-MS $[M]^+$ calcd. for ($C_{88}H_{108}Br_2N_8O_2S_3$): 1564.6104; found: 1564.6136.

Synthesis of BTP-T2F

In a 50 mL three neck flask, add compound 5 (140 mg, 89.41 μmol), compound 6 (39.85 mg, 89.41 μmol), $Pd_2(dba)_3$ (2.45 mg, 2.68 μmol), $P(o\text{-}tol)_3$ (3.27 mg, 10.73 μmol) and toluene (3.0 mL). Stir at 110 ^oC for 72 h under argon atmosphere. After cooling down, wash the mixture with methanol. The low molecular weight fraction was removed using Soxhlet extraction with methanol, hexane, acetone and dichloromethane, sequentially. Soxhlet extract with chloroform, extract and wash in methanol to afford BTP-T2F as black solid (61 mg, 45%).

Synthesis of BTP-2T2F

In a 50 mL three neck flask, add compound 5 (150 mg, 95.79 μmol), compound 7 (50.56 mg, 95.79 μmol), $Pd_2(dba)_3$ (2.63 mg, 2.87 μmol), $P(o\text{-}tol)_3$ (3.50 mg, 11.49 μmol) and toluene (3.0 mL). Stir at 110 ^{o}C for 72 h under argon atmosphere. After cooling down, wash the mixture with methanol. The low molecular weight fraction was removed using Soxhlet extraction with methanol, hexane, acetone and dichloromethane, sequentially. Soxhlet extract with chloroform, extract and wash in methanol to afford BTP-2T2F as black solid (77 mg, 50%).

3. References

[1] K. J. Kass, M. Forster, U. Scherf, *Angew. Chemie Int. Ed.* **2016**, *55*, 7816.

[2] Z. Luo, T. Liu, R. Ma, Y. Xiao, L. Zhan, G. Zhang, H. Sun, F. Ni, G. Chai, J. Wang, C. Zhong, Y. Zou, X. Guo, X. Lu, H. Chen, H. Yan, C. Yang, *Adv. Mater.* **2020**, *32*, 2005942.

4. Supporting Figures

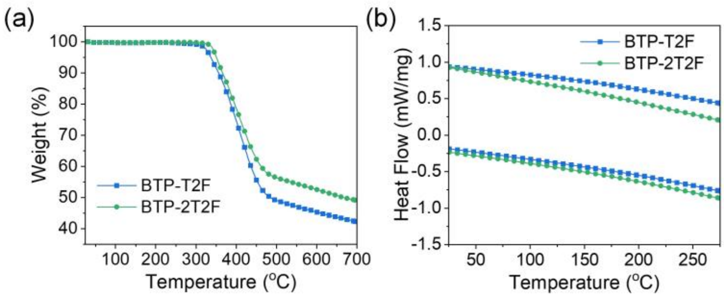

Figure S1. TGA (a) and DSC (b) of the two BTP-based polymers

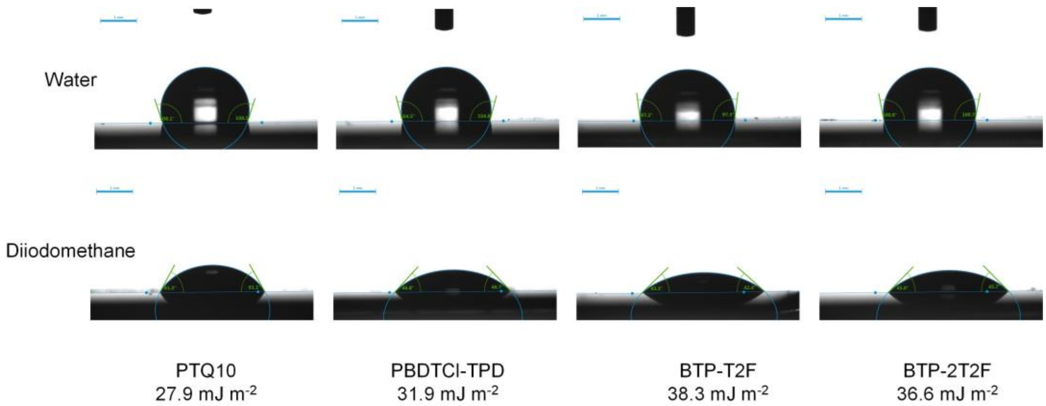

Figure S2. Surface energy measurements for the polymer semiconductors used in this work.

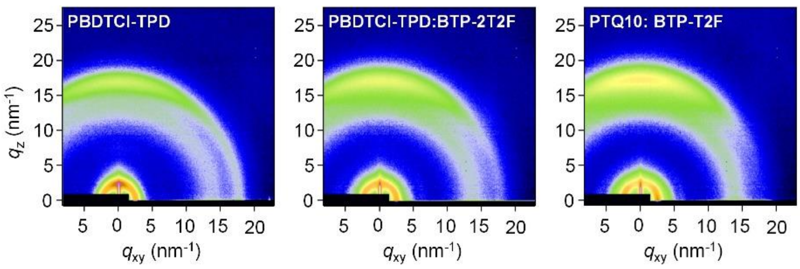

Figure S3. GIWAXS images of neat and blended polymer thin films.

TOC

Cost-Efficiency Balanced Polymer Acceptors Based on Lowly Fused Dithienopyrrolo[3, 2b]benzothiadiazole for 16.04% Efficiency All-Polymer Solar Cells

Chentong Liao,[a] Yufei Gong,[a] Xiaopeng Xu,[a] Liyang Yu,[a] Ruipeng Li,[b] and Qiang Peng[a]**

[a] School of Chemical Engineering, Key Laboratory of Green Chemistry and Technology of Ministry of Education and State Key Laboratory of Polymer Materials Engineering, Sichuan University, Chengdu 610065, P. R. China

[b] National Synchrotron Light Source II, Brookhaven National Lab, Suffolk, Upton, NY 11973, USA

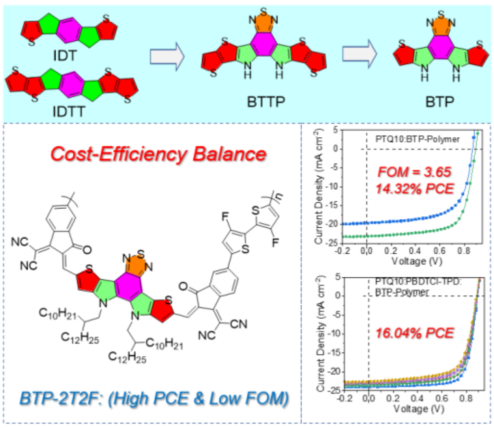

Dithienopyrrolo[3, 2b]benzothiadiazole (BTP)-based polymer accepters with low-lying HOMO level and reduced synthesis complexity compared to Y6-based polymer acceptors were developed for all polymer solar cells. Top PCEs of 14.32% and 16.04% were achieved in binary and ternary blends using BTP-based polymer acceptor, even featuring a very low FOM of 3.65.